Materials Research. 2024; 27(suppl. 1):e20240075
DOI: https://doi.org/10.1590/1980-5373-MR-2024-0075

Superhydrophobic Nanocoatings on Galvanized Steel and Aluminum: Enhancing Oil & Gas Sustainability

***Maria Isabel Collasius Malta*[a*], *Hugo Antonio Cavalcanti e Silva*[a],**

***Paulo Roberto Sá de Oliveira Neto*[a], *Rafael Gleymir Casanova da Silva*[b],**

***Walter Leandro Cordeiro da Silva Filho*[a], *Jedaías Januário da Silva*[a],**

***Severino Leopoldino Urtiga Filho*[a], *Magda Rosângela Santos Vieira*[a]**

[a]*Universidade Federal de Pernambuco, Departamento de Engenharia Mecânica, Avenida Professor Moraes Rego, 1235, Cidade Universitária, 50670-901, Recife, PE, Brasil.*
[b]*Universidade Federal de Pernambuco, Departamento de Engenharia Química, Avenida Professor Moraes Rego, 1235, Cidade Universitária, 50670-901, Recife, PE, Brasil.*

Received: February 16, 2024; Revised: May 19, 2024; Accepted: May 23, 2024

Superhydrophobic surfaces offer innovative solutions, particularly in water/oil separation systems, as they repel water and attract oil, enabling efficient separation. The study aimed to analyze coatings developed on galvanized steel and aluminum, regarding their wettability in saline water and diesel oil, aiming for applications in the oil and gas industry. Specimens underwent texturizing, in-situ growth of layered double hydroxide (ZnAl-LDH) film and modification with stearic acid (STA). Both LDH films exhibited similar binary hierarchical structures of hexagonal petals and micrometric flowers, interconnecting along the surface, forming pores that allowed for air entrapment after STA modification. CA for saline water exceeded 150º, and for diesel oil was under 10º, characterizing the coatings as superhydrophobic and superoleophilic. The coatings show promising potential for water/oil separation using recyclable substrates and a simple, low-cost, environmentally friendly process.

Keywords: *Nanocoatings, LDH films, Superoleophilicity, Superhydrophobicity, Water/oil Separation.*

1. Introduction

The oil and gas sector is one of the main drivers of the global economy. In 2021, global investment in oil and gas exploration was more than US$30 trillion. In the same year, Brazil achieved a record-breaking oil export of approximately US$31 billion, generating a revenue of R$104 billion in taxes, deductions and fees[1].

Unfortunately, accidents and environmental disasters associated with this sector have been documented in Brazil since 1975[2,3], often related to significant oil spills. Highlights include the accident in Guanabara Bay (RJ) in 1997, with a spill of 2.8 million liters of fuel oil into mangroves[4], the 2019 incident along the Brazilian coast affecting over 9 states with the appearance of crude oil; and a similar event in 2022, on the coast of Ceará state, proving how the problem remains current[5].

Wettability is a property of materials related to the interaction of a liquid with a solid surface, being influenced by both morphology and chemical composition. With water and oil being chemically opposite, surfaces typically exhibit completely different wettability behaviors. In other words, a surface that repels water tends to attract oil, and vice versa[6,7].

Water/oil-repellent coatings have a wide range of applications in the oil and gas industry. They can be used to extend the lifespan of offshore platforms by mitigating corrosive and fouling processes and enhance the flow and efficiency of pipelines by reducing drag and minimizing scale formation. In processing equipment, these coatings can improve the effectiveness of refining processes by acting as water-oil separators. Additionally, they can be applied to oil-water separation meshes to minimize the environmental impact of oil leaks[8,9].

The Brazilian company Petrobras' strategic plan establishes an ambitious goal of zero leaks by 2028[10]. To achieve this goal, the prevention - and appropriate response - to accidents is extremely important. In this context, the search for innovation and the adoption of new solutions plays a crucial role. Superhydrophobic (SHP) surfaces emerge as a promising solution, arousing the interest of researchers due to their numerous application possibilities, including their use in water/oil separation systems[11,12].

Quantitatively, the most common method for determining wettability is measuring the contact angle (CA). A SHP surface (CA ≥ 150°), which repels water, often exhibits the opposite behavior with oil, causing the liquid to spread (CA < 10°), and vice versa[13-15]. This characteristic allows for more efficient separation of these two liquids[9], enabling the creation of three different types of materials: those that remove water[7,16], those that remove oil[8], or those that alter under control[17,18].

*e-mail: mariaisabelcollasiusmalta@gmail.com

One method to achieve such surfaces involves the combination of double-layered hydroxide films and fatty acids[19,20]. These compounds are characterized by the formula $[M^{2+}_{1-x}M^{3+}_{x}(OH)_2]^{x+}.(A^{n-})_{x/n}.yH_2O$, where M^{2+} e M^{3+} represent metal cations in lamellar structures with a A^{n-} anion located in the interlayer space. Due to the flexibility in modifying their composition, various chemical combinations can be generated, making them extensively utilized for creating SHP surfaces[21-23]. They serve as agents for aggregating roughness and aiding in compatibility with surface energy-reducing agents, given their richness in hydroxyl groups[24,25]. The main objective is to form a hierarchical micro/nanometric structure, generating air pockets beneath droplets and achieving larger contact angles, following the Cassie-Baxter wettability model[26,27]. Figure 1 illustrates the interaction between a droplet and a rough surface according to the Cassie-Baxter wettability model (Fig. 1a) and in the presence of a modified LDH film (Fig. 1b).

Efficient oil-water separation not only contributes to environmental protection but also addresses industrial pollution from oily wastewater, aligning with sustainable development goals[28,29]. Given this, and in accordance with the SDGs, this work aims to analyze and characterize coatings on galvanized steel and aluminum 5052 substrates regarding their wettability with water and diesel, aiming for potential applications in oil-water separation.

2. Experimental

2.1. Materials

Aluminum alloy 5052 was supplied by Metaltorque Metais e Ferramentas Ltd. Galvanized A35 steel was provided by Galvanisa Ltd. Zinc nitrate hexahydrate ($Zn(NO_3)_2 \cdot 6H_2O$) and aluminum nitrate nonahydrate ($Al(NO_3)_3 \cdot 9H_2O$) was procured from Dinâmica Química Contemporânea Ltd. Isopropyl/ethanolic alcohol and hydrochloric acid (HCl) were obtained from Anidrol Produtos para Laboratório Ltd. Ammonium hydroxide (NH_4OH) and acetone were sourced from Química Moderna Indústria e Comércio Ltd. Sodium chloride (NaCl) was acquired from Hexis Científica Ltd. Diesel fuel was obtained from a local gas station. All reagents were of analytical grade and utilized without additional purification.

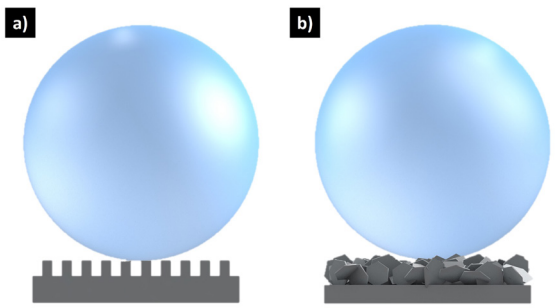

Figure 1. Interaction of a water droplet based on the Cassie-Baxter wettability model (a) and on a modified LDH film (b).

2.2. Preparation of specimens and surface treatment

The AA5052 (Al) samples were initially cut into dimensions of (20 x 20 x 3) mm, followed by a sanding process up to #1200 grit to remove oxides and homogenize the surface. The final step involved an acid attack in HCl (2M) for 10 minutes, aiming to create an initial microstructure.

The galvanized steel (GS) samples were supplied pre-cut and industrially coated, with dimensions of (30 x 30 x 6) mm. Surface treatment for these samples involved a light blasting with alumina to remove oxides present on the surface and create a more uniform initial texture.

The surface preparation process was followed by cleaning with isopropyl alcohol and acetone in an ultrasonic bath for 5 minutes each, followed by air drying.

2.3. Chemical modifications

The creation of the suitable morphology for achieving superhydrophobicity was accomplished through the development of films of Zn-Al layered double hydroxide (LDH). The Zn-Al-LDH coatings were generated in-situ on aluminum and galvanized steel surfaces, alternating the suppliers of Al^{3+} e Zn^{2+} cations between the substrate and nitrate solutions.

Al samples (Al^{3+} source) were modified in a zinc nitrate solution (Zn^{2+} source), while GS samples (Zn^{2+} source) were modified in an aluminum nitrate solution (Al^{3+} source). Both modifications were carried out in a water bath for 180 minutes at 70°C in a 0.1M solution in the presence of ammonia.

The surfaces were then modified with a surface energy-reducing agent to achieve water repellency. This process involved immersion in a stearic acid solution (1% w/v) for 90 minutes. Finally, the surfaces were placed in an oven where they remained for 120 minutes at 80 °C, before being cooled at room temperature (25°C).

2.4. Surfaces characterization

2.4.1. Topography and roughness parameters

The topography and roughness parameters, including (Ra), root mean square (RMS), skewness (Rsk), and kurtosis (Rku), were analyzed using a confocal microscope (Zeiss – Axio Imager Z2m).

2.4.2. Morphological and chemical characterization

For surface morphology evaluation, a Field Emission SEM was utilized (Tescan – MIRA 3, Mira TC software). Additionally, a semi-qualitative chemical analysis was performed using EDS (Oxford Instruments – X-act 51-ADD007, Aztec software) associated with the SEM.

2.4.3. Zinc layer thickness

The measurement of the coating layer thickness was performed by taking five random measurements on each side of the galvanized steel sample using a thickness gauge (DeFelsko® – Positector® 6000 series).

2.4.4. Wettability

The wettability of the surfaces was assessed through contact angle measurements using an optical goniometer

(Biolin Scientific® Theta Attention®, OneAttension 3.0 software). The measurements were conducted at room temperature (25°C) with an average of 5 drops of saline water (NaCl 3,5%) and diesel (10 µl) randomly dispensed along the surface.

3. Results and Discussions

3.1. Topography and roughness parameters

The achievement of superhydrophobicity on solid surfaces relies on the combination of a micro-nanometric structure and low surface energy[30,31]. Therefore, to establish an initial roughness for anchoring the Zn-Al-LDH films, preliminary texturizing processes were implemented on the surfaces of both the aluminum (Al) and galvanized steel (GS) samples. Table 1 shows the roughness parameters before and after the initial texturization.

Rq (Root Mean Square) represents the standard deviation of surface heights, serving as a parameter less susceptible to extreme values in the measurement[32]. A significant increase in the RMS value was observed from the sanded Al sample to the etched one, indicating that the chemical etching induced a heightened roughness on the surface, as confirmed in the 3D surface images (Figure 2a and 2b). The color-coded topography histogram visually demonstrates a threefold increase in the total profile amplitude, from 60 to 180 um.

SEM images show how the acid etching applied to the Al samples altered the surface morphology, evolving from parallel scratches (Fig. 2.a1), typical of the sanding process with abrasive paper, to interconnected micrometric structures arranged in a cubic-like[33] pattern with smooth tops (Fig. 2.a2). This transformation is attributed to the selective action of HCl in regions around the dislocations, resulting in the formation of micropits through the reactions[34-36]:

$$Al_2O_3 + 6HCl \rightarrow 2AlCl_3 + 3H_2O \quad (1)$$

$$2Al + 6HCl \rightarrow 2AlCl_3 + 3H_2 \quad (2)$$

The specialized roughness parameters, Rsk and Rku, serve as indicators of asymmetry and sharpness of irregularities, respectively. Rsk values < 0 signify a prevalence of irregularities with heights below the average, while Rku values > 3 indicate that more pronounced irregularities are concentrated on the surface (leptokurtic)[32]. Despite the complete alteration of surface morphology through HCl etching, the Rsk and Rku values of the texturized Al remained nearly unaltered. This suggests that the surface continued to maintain a prevalence of narrow valleys, with irregularities proportionally increased in both directions.

Due to zinc's high susceptibility to HCl acidic etching[37], texturization was achieved through light alumina blasting. SEM images of the untreated GS (Fig. 2.b1) displays ridges associated with the cooling process of molten zinc and the presence of corrosion products. The blasting process induced a structure of multidirectional scratches (Fig. 2.b2) with coarser dimensions compared to the etched aluminum surface. Contrastingly to the Al sample, the blasted GS sample exhibited a slight decrease in RMS, as blasting is a common procedure for eliminating irregularities or contaminants[38], besides establishing an anchor profile.

Simultaneously, the analysis of the color histogram reveals an unaltered total profile amplitude of the surface. This outcome suggests that texturization modified the morphology of existing irregularities without impacting the total profile height, which remained at 55 µm. In fact, the

Table 1. Roughness parameters before and after texturization.

	Sanded Al	Etched Al	Untreated GS	Blasted GS
Ra	1.153	4.890	2.305	1.709
Rq	1.497	6.672	2.707	2.157
Rsk	-0.345	-0.358	-0.658	-0.149
Rku	5.237	5.680	2.304	4.012

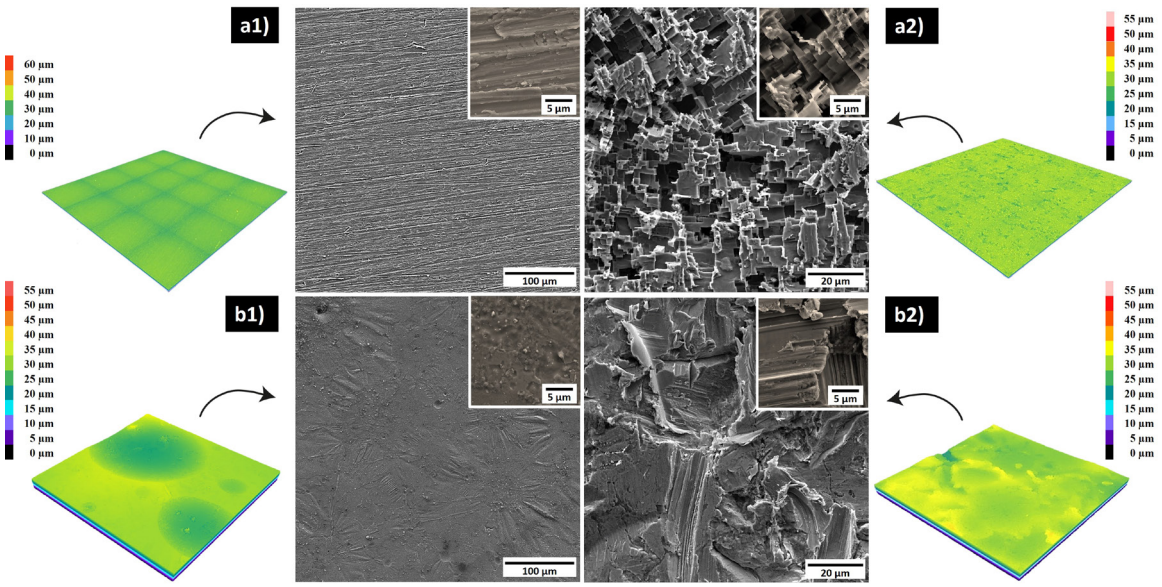

Figure 2. SEM and topographic analysis of substrate surfaces: (a1) Sanded Al, (a2) HCl etched Al, (b1) Untreated GS, and (b2) Blasted GS.

obtained roughness parameters indicate that blasting caused a slight decrease in Rq, albeit not significantly pronounced. Despite the increase in the Rsk value, implying a tendency to form peaks along the surface, the sample maintained a prevalence of valleys (Rsk < 0). Rku indicates that the existing irregularities became sharper after blasting, aligning with the SEM images.

3.2. Zinc layer thickness

To assess material loss and financial viability, the Al and GS samples were weighed before and after the acid etching and blasting procedures, respectively. The data indicated a loss of less than 1.5% for Al and 1% for GS. However, for the GS samples, evaluating the loss of thickness is also crucial to evaluate the impact on the barrier protection of the coating.

The Brazilian technical standard NBR-6323 stipulates a minimum zinc layer thickness of 84 µm in the galvanization process for steel products[39]. The zinc layer of industrially galvanized samples measured approximately 91 µm, complying with the technical standard. However, the blasting process resulted in a reduction of about 10% in thickness (averaging 9 µm), making the coating slightly below the specified value. Consequently, the blasting process carried out needs to undergo modifications in the future to avoid compromising the corrosion protection of the steel, as the operational conditions of the oil and gas industry in Brazil are known to subject steel products to harsh environmental challenges[40-42].

3.3. Morphological and chemical characterization

The Zn-Al-LDH film was designed to alter the textured surface of GS and Al, creating a micro-nano-hierarchical geometry that facilitates the entrapment of air beneath the droplet. The in-situ formation of the films included the dissolution of the substrates, utilizing them as a source of bivalent cations (Zn^{2+}) for galvanized steel and trivalent cations (Al^{3+}) for the aluminum alloy. The missing metallic cations in both cases were provided by the precursor salts, aluminum nitrate, and zinc nitrate, respectively.

Figure 3 provides a comparison between the microscopies of the LDH films obtained on the two substrates: (a) Al and (b) GS. In both samples, it is possible to observe the deposition of lamellar structures in the form of hexagonal petals that cluster together to form hierarchical micro-nanostructures resembling flowers. The vertical alignment of these lamellae creates an interconnected network that allows the formation of pores throughout the entire surface. These characteristics of the LDH films contribute to an increase in the surface area, as well as to achieving a wettability configuration similar to the Cassie-Baxter model[43-45].

Comparing Figures (3a1 and 3b1) with Figures (3a2 and 3b2) reveals that the LDH film on the GS substrate exhibited more refined lamellae with a denser presence on the substrate, forming smaller flowers (highlighted). The presence of clear nanorods clustered in star-like shapes was only observed in the Al sample, being associated with zinc oxide (ZnO)[44,45].

The enlarged images provide a clearer view of the flower-like structures (Figures 3a3 and 3b3). The lamellae thickness on the AA5052 substrate ranged from 100 to 200 nm, while on the galvanized substrate, it varied from 52 to 76 nm. The images highlight a greater number of pores for the LDH on the galvanized substrate, a morphological feature that, as previously mentioned, may contribute to improving water repellency properties.

The elemental composition analysis of both GS and Al samples (Figure 4) reveals significant alterations induced

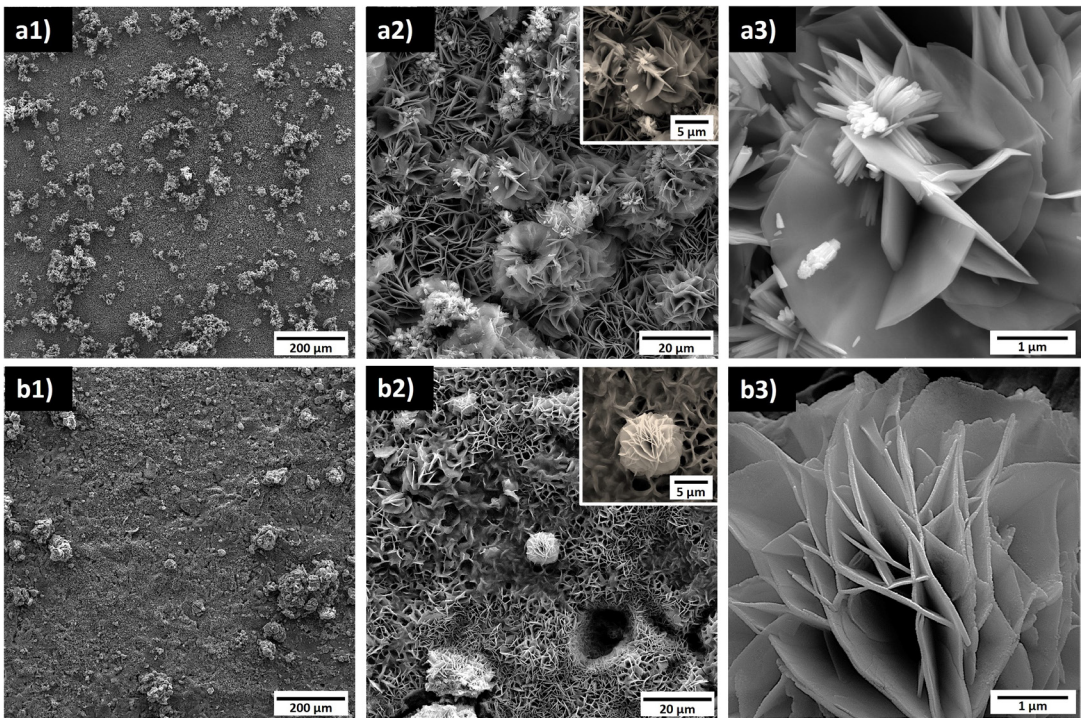

Figure 3. Surface morphologies revealed by SEM: (a) Al substrate and (b) GS substrate.

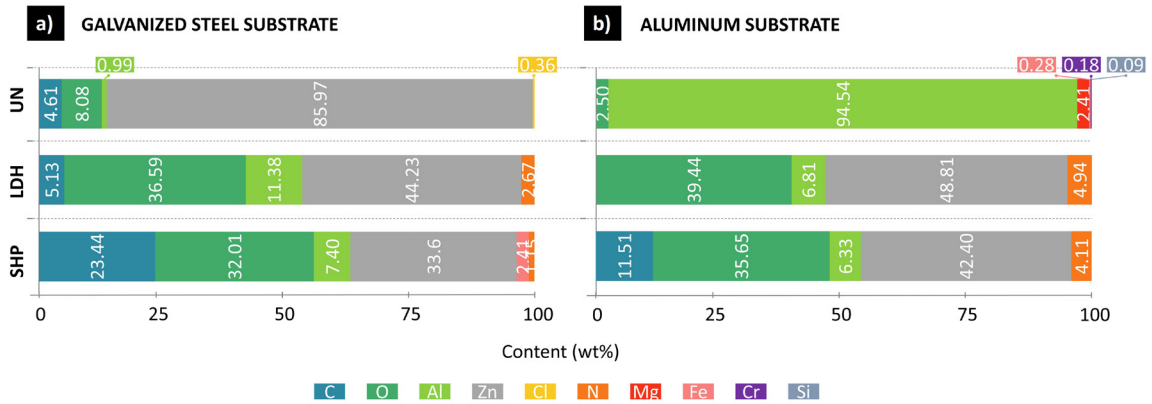

Figure 4. Elemental composition analysis of samples: (a) GS and (b) Al.

by the in-situ formation of the Zn-Al-LDH film. In the GS sample (Figure 4a), the conversion coating introduced the element N to the untreated surface (UN). Notably, there is an increase in the O and Al elements, coupled with a decrease in the Zn element. This observed behavior can be linked to the LDH film formation process, which obtained external Al^{3+} cations through aluminum nitrate, while the only source of Zn^{2+} was derived from the substrate being coated. The presence of C element in the composition may be attributed to the existence of zinc carbonate on the surface.

A similar trend was observed for the Al sample (Figure 4b). The chemical modification resulted in the appearance of new elements, including N and Zn, not originally present in the substrate (UN). Additionally, the alloying elements and impurities inherent in the substrate, such as Mg, Si, and Cr, remained unidentified, suggesting the occurrence of surface coating. Analogous to the GS sample, the concentration of the metallic cation supplied by the substrate (Al^{3+}, in this case) was reduced and the O element exhibited a significant increase.

Thus, the coatings obtained in the GS and Al samples showed similar proportions of the elements O, Zn, Al, and N, which constitute the main elements of a Zn-Al-LDH film.

The high concentration of O element plays a crucial role in the formation of Zn-Al-LDH films as it is present in the hydroxide ions (OH^-) within the lamellae. These ions react with the metallic cations, forming Al and Zn hydroxides[44]. This chemical reaction contributes to facilitates the interaction with fatty acids (in addition of the increased surface area provided by the LDH films), as the hydroxides bind with the polar carboxyl group of these fatty acid[31,44,45].

The Figure 4 also illustrates the changes in chemical composition after stearic acid coating. There is an increased presence of carbon in the GS sample (Figure 4a) and its emergence in the Al sample (Figure 4b). These chemical alterations manifest in the SEM images (Figure 5 a1 and b1), showcasing a translucent deposition on both substrates. Through EDS mapping of the C element (Figure 5 a2 and b2), this deposition is linked to the stearic acid molecule, while retaining the hierarchical structure previously established during the formation of LDH films.

Stearic acid is a long-chain carboxylic acid with 18 carbon atoms in its structure. At one end of its chain, the presence of the carboxyl group (-COOH) allows this compound to react with the LDH film (OH^-) through an acid-base reaction, resulting in the formation of carboxylate ions and water (Figure 6a). Following this reaction, the carbon chain (nonpolar) of the formed carboxylate ion is oriented opposite to the substrate, as depicted in Figure 6b[25,31,44].

3.4. Wettability

The interaction between the Zn-Al-LDH films and the fatty acid can be more effectively evaluated by examining the evolution of surface wettability. Typically, metal surfaces are hydrophilic, characterized by contact angles (CA) of less than 90° 28. As expected, the untreated Al presented a hydrophilic wettability with CA_{UN} =70°. However, untreated GS was hydrophobic, with CA_{UN} =107°. Texturing the surface, as explained by Wenzel, enhances the intrinsic wettability of the material. This behavior was indeed observed on the etched Al and blasted GS, where the initial CA dropped to 52° for Al and to 89° for GS. Figure 7 depicts a graph illustrating the progression of CA throughout the process of achieving nanometric coatings on Al and GS samples.

The abrupt change in wettability occurs when the LDH film is formed, transforming the surfaces into super-hydrophilic due to the presence of hydrophilic groups (hydroxide ions)[15], as presented in Figure 6a. The contact angles of both Zn-Al-LDH films were found to be close to zero.

The modification with the surface energy agent allows to alter the wettability of the samples from super-hydrophilic to superhydrophobic, as shown in Figure 7. CA values for GS and Al both increased from 0° to CA values exceeding 150°, rendering the surfaces highly water-repellent and minimizing the contact between the liquid and the solid.

The reduction in contact can be quantified using the Cassie-Baxter formula (Equation 1), which calculates the portion of air retained between the water droplet and the coating. This approach allows for the quantification of the water repellency efficiency of the substrate, as a greater amount of air beneath the droplet implies less contact with the substrate. Equation 3 is described below:

$$\mathrm{Cos}\theta_{SHP} = fs\left(\cos\theta_{SMOOTH} + 1\right) - 1 \quad (3)$$

where fs denotates the solid fraction, θ_{SHP} corresponds to the coating CA value, and θ_{SMOOTH} represents the CA of an ideal surface of the same material[46,47]. The contact angles for the smooth surfaces of Al and GS, modified only with AE, were

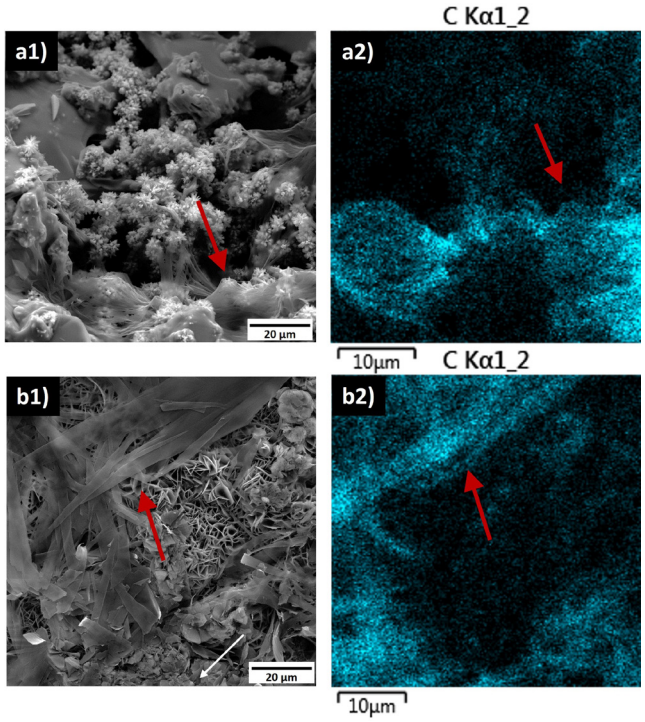

Figure 5. SEM images (1) and EDS mapping of Carbon element (2) after stearic acid modification of Zn-Al-LDH films on (a) Al and (b) GS samples.

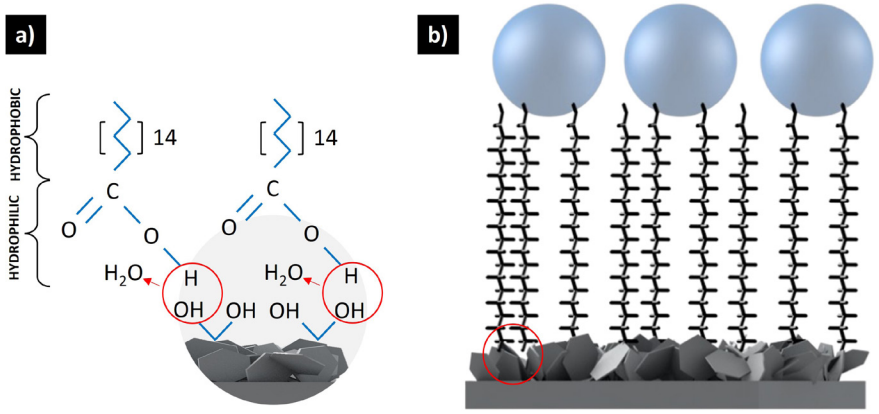

Figure 6. Schematic representation of Zn-Al-LDH and stearic acid interaction.

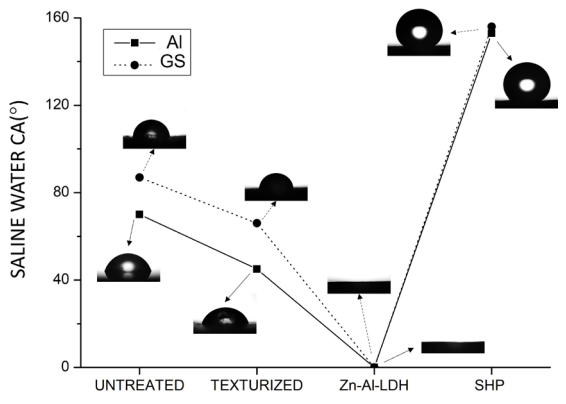

Figure 7. Contact angle evolution during nanometric coating formation in GS and Al samples.

103° and 110º, respectively. Thus, the air fraction (1-fs) for the SHP coatings of Al and GS is 86% and 87%, respectively. This means that the contact between the electrolyte and the metallic surface is reduced to less than 15% in both samples.

This outcome is visually manifested by the emergence of an air layer when the SHP surfaces are completely submerged in water. In Figure 8, both the uncoated and SHP-coated Al and GS samples were submerged in a synthetic seawater solution. While Figures 8.a1 and 8.b1 depict the uncoated samples as opaque, Figures 8.a2 and 8.b2 display a distinctive gleam, or silvery shine, indicative of the Salvinia Effect. This phenomenon occurs from the total reflection of incident light at the air-water interface[48,49].

Scientists explain that a surface showcasing the Salvinia Effect, upon encountering an oil film on a water surface, ends up adsorbing it[49-51]. This behavior is attributed to the

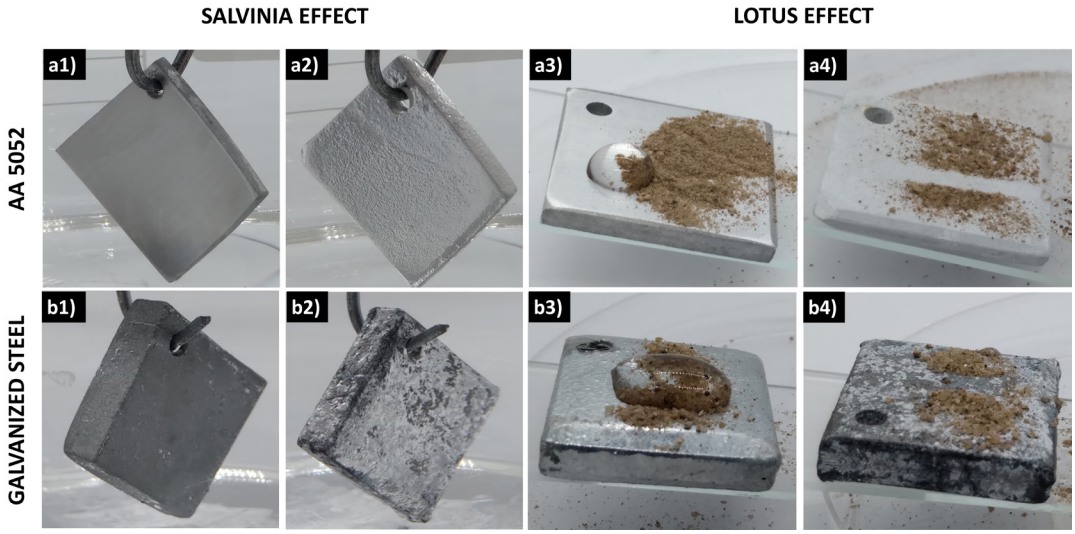

Figure 8. Salvinia and lotus effects on Al (a) and GS samples (b): uncoated (1 and 3) and superhydrophobic (2 and 4).

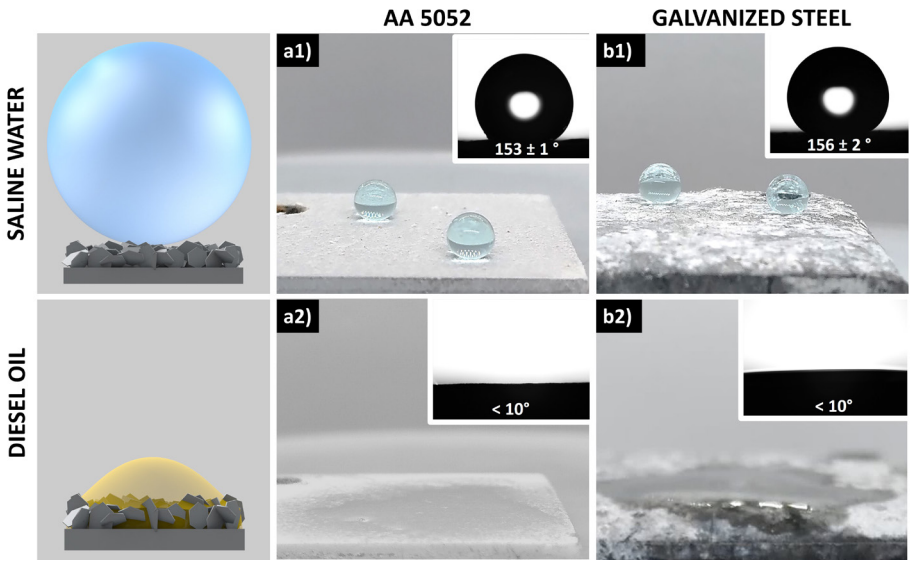

Figure 9. Wettability of nanometric coatings on (a) Al and (b) GS samples with saline water and diesel oil.

infiltration of oil into the hierarchical structures of the surface, replacing the pre-existing air. Therefore, the substantial air content within the coatings obtained on Al and GS substrates suggests a promising application as a solution for oil spills along the Brazilian coastline[52].

The Lotus effect, denoting the self-cleaning attribute of SHP coatings, was assessed in Figure 8b. Both uncoated and SHP-coated samples were tilted at a 10° angle, with sand grains placed on their surfaces. Self-cleaning is a significant characteristic as dirt can negatively impact the interaction between water and the surface, thus affecting the efficiency of oil/water separation. In the case of uncoated samples (Figures 8a3 and 8b3), dirt resists removal by the droplet, remaining on the surface where the droplet exhibits high adhesion. In contrast, the SHP surfaces of Al (Figure 8a4) and GS (Figure 8b4) effectively removed dirt as the droplet rolled, leaving behind a clean trail on the surfaces.

Superhydrophobic coatings, as explained previously, tend to demonstrate strong interaction with oily compounds, presenting oleophilic tendencies that extend to superoleophilic behavior[13-15,53]. In Figure 9, photographs of water and diesel oil droplets on the SHP coatings obtained on the AA5052 aluminum alloy and galvanized steel are presented.

As observed, the coatings applied to aluminum (Fig. 9.a2) and galvanized steel (Fig. 9.b2) exhibited contact angles with diesel oil of less than 10°, indicating extensive spreading of the droplet and high wetting of the surface by the oil.

This observed superoleophilic behavior can be attributed to the presence of aluminum stearate and zinc stearate compounds, respectively formed on the surfaces of the aluminum alloy and galvanized steel[31,44]. As previously represented in Figure 6, the stearate of the corresponding metal has a long carbon chain (18 carbons), which is oriented towards the outer part of the coating. Thus, this long chain,

having a nonpolar character, promotes water repellency, which has a polar nature and allows significant interaction with diesel oil, which has a nonpolar character[54,55].

4. Conclusions

The obtained coatings have demonstrated significant potential for application in mitigating and controlling oil leakage contamination in natural waters. The Zn-Al-LDH films, derived from different sources of metal cations Zn^{2+} and Al^{3+}, produced similar petal and flower-like structures, enhancing the surface area, and forming numerous pores across the surface. Finer structures were observed on the galvanized steel substrate, resulting in a higher quantity of pores and increased adsorption of the carbon element, present in the surface energy-reducing agent. Stearic acid chemically interacted with the LDH films, modifying the wettability of the surfaces from superhydrophilic to superhydrophobic. Both coatings exhibited the Lotus Effect, indicating a low interaction between the surfaces and the droplets, as predicted by the Cassie-Baxter wetting model. Additionally, the Salvinia Effect, also identified in both samples, suggests that the micro-nanometric hierarchical structures formed by the Zn-Al-LDH film created a texture capable of forming air pockets upon interaction with water. In contrast, when encountering oil, which possesses polarity opposite to that of water, these air pockets functionated as fluid reservoirs, effectively adsorbing the liquid. As a result, superhydrophobic and superoleophilic coatings have been attained, exhibiting mutual repellency to water and absorption of oil. Therefore, these coatings represent a promising and sustainable alternative for the development of meshes, networks, and/or separation membranes for these fluids, which can address industrial and environmental challenges through a simple, cost-effective, and environmentally friendly approach.

5. Acknowledgments

This study was carried out at the Federal University of Pernambuco/Brazil, inside the National Institute of Technology in Union and Materials Coating (INTM), the Laboratory of Composite Materials and Structural Integrity (LBC-CompoLAB), and the Research Institute in Petroleum and Energy (LITPEG). The Financier of Studies and Projects (Finep), the National Agency for Petroleum, Natural Gas, and Biofuels (ANP), the Pernambuco State Support Foundation for Science and Technology (FACEPE), the National Council of Scientific and Technological Development (CNPq), and the Coordination for the Improvement of Higher Education Personnel (CAPES) have all provided funding for this research.

6. References

1. Silva EB Fo, Oliveira JM, Araújo BCPO. Eficiência produtiva: análise e proposições para aumentar a produtividade no Brasil. Brasília: Ipea; 2023.
2. Tiburtius ERL, Peralta-Zamora P, Leal ES. Contaminação de águas por BTXs e processos utilizados na remediação de sítios contaminados. Quim Nova. 2004;27(3):441-6.
3. Pereira AFDAN, Quelhas OLG. Os acidentes industriais e suas consequências. In: 4th International Conference On Industrial Engineering and Industrial Management/XIV Congreso de Ingeniería de Organización; 2009 September 08-10; Donostia- San Sebastián, España. Proceedings. Basque Country: ADINGOR; 2010. p. 652-61.
4. Fonseca IL, Oliveira WA. Desastres socioambientais, turismo e resiliência: reflexões sobre o vazamento de óleo na costa do Nordeste do Brasil. RTA. 2021;32(1):120-40.
5. Azevedo RNA. Caracterização da impressão digital do óleo derramado no litoral cearense em 2019 e 2022 usando técnicas analíticas de alta resolução. Uma abordagem geoquímica ambiental forense [dissertation]. Fortaleza: Federal University of Ceará; 2023.
6. Jeevahan J, Chandrasekaran M, Joseph GB, Durairaj RB, Mageshwaran G. Superhydrophobic surfaces: a review on fundamentals, applications, and challenges. J Coat Technol Res. 2018;15(2):231-50.
7. Zhao L, Du Z, Tai X, Ma Y. One-step facile fabrication of hydrophobic SiO2 coated super-hydrophobic/super-oleophilic mesh via an improved Stöber method to efficient oil/water separation. Colloids Surf A Physicochem Eng Asp. 2021;623(24):126404.
8. Hu J, Zhan Y, Zhang G, Feng Q, Yang W, Chiao YH, et al. Durable and super-hydrophilic/underwater super-oleophobic two-dimensional MXene composite lamellar membrane with photocatalytic self-cleaning property for efficient oil/water separation in harsh environments. J Membr Sci. 2021;637(1):119627.
9. Usman J, Othman MHD, Ismail AF, Rahman MA, Jaafar J, Raji YO, et al. An overview of superhydrophobic ceramic membrane surface modification for oil-water separation. J Mater Res Technol. 2021;12(12):643-67.
10. Petrobrás. Plano Estratégico: novos movimentos, pés no presente e olhos no futuro [Internet]. Rio de Janeiro: Petrobrás; 2024 [cited 2024 Feb 14]. Available from: https://www.petrobras.com.br/quem-somos/estrategia
11. Fu C, Gu L, Zeng Z, Xue Q. One-step transformation of metal meshes to robust superhydrophobic and superoleophilic meshes for highly efficient oil spill cleanup and oil/water separation. ACS Appl Mater Interfaces. 2019;12(1):1850-7.
12. Khosravi M, Azizian S, Boukherroub R. Efficient oil/water separation by superhydrophobic CuxS coated on copper mesh. Separ Purif Tech. 2019;215:573-81.
13. Yong J, Huo J, Chen F, Yang Q, Hou X. Oil/water separation based on natural materials with super-wettability: recent advances. Phys Chem Chem Phys. 2018;20(39):25140-63.
14. Chen C, Weng D, Mahmood A, Chen S, Wang J. Separation mechanism and construction of surfaces with special wettability for oil/water separation. ACS Appl Mater Interfaces. 2019;11(11):11006-27.
15. Ma Z, Liang S, Zhang S, Xiao K, Wang X, Li M, et al. Surface functionalization via synergistic grafting of surface-modified silica nanoparticles and layered double hydroxide nanosheets for fabrication of superhydrophilic but relatively oleophobic antifouling membranes. Separ Purif Tech. 2020;247:116955.
16. Rasouli S, Rezaei N, Hamedi H, Zendehboudi S, Duan X. Design, fabrication, and characterization of a facile superhydrophobic and superoleophilic mesh-based membrane for selective oil-water separation. Chem Eng Sci. 2021;236:116354.
17. He S, Zhan Y, Bai Y, Hu J, Li Y, Zhang G, et al. Gravity-driven and high flux super-hydrophobic/super-oleophilic poly (arylene ether nitrile) nanofibrous composite membranes for efficient water-in-oil emulsions separation in harsh environments. Compos, Part B Eng. 2019;177(15):107439.
18. Liu L, Pan Y, Jiang K, Zhao X. On-demand oil/water separation enabled by magnetic super-oleophobic/super-hydrophilic surfaces with solvent-responsive wettability transition. Appl Surf Sci. 2020;533:147092.
19. Kalusulingam R, Koilraj P, Antonyraj CA, Srinivasan K. Recent advances on the fabrication of superwettable layered double hydroxides materials for oil–water separation. Mater Today Proc. 2023. In press.

20. Cao H. Low adhesive and superhydrophobic LDH coating for anti-corrosion and self-cleaning. Colloids Surf A Physicochem Eng Asp. 2022;652:129893.
21. Zhu YX, Song GL, Wu PP, Huang JF, Zheng DJ. A protective superhydrophobic Mg–Zn–Al LDH film on surface-alloyed magnesium. J Alloys Compd. 2021;855:157550.
22. Aladpoosh R, Montazer M. Functionalization of cellulose fibers alongside growth of 2D LDH platelets through urea hydrolysis inspired Taro wettability. Carbohydr Polym. 2022;275:118584.
23. Kalusulingam R, Nataraj SK, Srinivasan K. Robust oil/water separation through super-wettable in-situ grown Si@ NiFe-LDH nanosheets on nickel foam. Mater Today Proc. 2023. In press.
24. Wang Z, Shen X, Qian T, Xu K, Sun Q, Jin C. Fabrication of superhydrophobic Mg/Al layered double hydroxide (LDH) coatings on medium density fiberboards (MDFs) with flame retardancy. Materials (Basel). 2018;11(7):1113.
25. Cao Y, Zheng D, Li X, Lin J, Wang C, Dong S, et al. Enhanced corrosion resistance of superhydrophobic layered double hydroxide films with long-term stability on Al substrate. ACS Appl Mater Interfaces. 2018;10(17):15150-62.
26. Iqbal MA, Asghar H, Fedel M. Ce-Doped-MgAl superhydrophobic layered double hydroxide for enhanced corrosion resistance properties. Solids. 2021;2(1):76-86.
27. Wang Y, Zhou X, Yin M, Pu J, Yuan N, Ding J. Superhydrophobic and self-healing Mg-Al layered double hydroxide/silane composite coatings on the Mg alloy surface with a long-term anti-corrosion lifetime. Langmuir. 2021;37(27):8129-38.
28. Yan T, Chen X, Zhang T, Yu J, Jiang X, Hu W, et al. A magnetic pH-induced textile fabric with switchable wettability for intelligent oil/water separation. Chem Eng J. 2018;347:52-63.
29. UNDP, IFC, IPIECA. Mapping the oil and gas industry to the sustainable development goals: an atlas. New York: UNDP; 2017.
30. Goswami A, Pillai SC, McGranaghan G. Micro/nanoscale surface modifications to combat heat exchanger fouling. Chemical Engineering Journal Advances. 2023;16:100519.
31. Silva RGC, Malta MIC, Carvalho LAP, Silva JJ, Silva WLC Fo, Oliveira SH, et al. Low-cost superhydrophobic coating on aluminum alloy with self-cleaning and repellency to water-based mixed liquids for anti-corrosive applications. Surf Coat Tech. 2023;457:129293.
32. Khaskhoussi A, Calabrese L, Patané S, Proverbio E. Effect of chemical surface texturing on the superhydrophobic behavior of micro–nano-roughened AA6082 surfaces. Materials (Basel). 2021;14(23):7161.
33. Kim K, Park HR, Kim HJ, Lee D, Ha S, Lee K, et al. Self-cleaning mechanisms according to the wettability of the surface and deposition material. Appl Surf Sci. 2023;626:157197.
34. Peng S, Bhushan B. Mechanically durable superoleophobic aluminum surfaces with microstep and nanoreticula hierarchical structure for self-cleaning and anti-smudge properties. J Colloid Interface Sci. 2016;461:273-84.
35. Wu R, Chao G, Jiang H, Hu Y, Pan A. The superhydrophobic aluminum surface prepared by different methods. Mater Lett. 2015;142:176-9.
36. Xiao X, Xie W, Ye Z. Preparation of corrosion-resisting superhydrophobic surface on aluminium substrate. Surf Eng. 2019;35(5):411-7.
37. Abbar JC, Swetha GA, Sachin HP. Impact of an expired hemorheologic drug on the mitigation of zinc corrosion in acidic environment: insights from chemical, electrochemical, and surface evaluation. Colloids Surf A Physicochem Eng Asp. 2022;650:129518.
38. Kamardin NK, Shah NHNEA, Ismail MH. Surface profile analysis: conventional blasting using garnet and recycled garnet. Proceedings of Mechanical Engineering Research Day. 2022;2022:253-4.
39. Associação Brasileira de Normas Técnicas. NBR ISO 4287: Especificações geométricas do produto (GPS) - Rugosidade: Método do perfil - Termos, definições e parâmetros da rugosidade. Rio de Janeiro: ABNT; 2002.
40. Oliveira ESDD, Pereira RFDC, Melo IRD, Lima MAGDA, Urtiga SL. Corrosion behavior of API 5L X80 steel in the produced water of onshore oil recovery facilities. Mater Res. 2017;20:432-9.
41. Beltrao RLC, Sombra CL, Lage ACV, Netto JRF, Henriques CCD. SS: pre-salt Santos basin-challenges and new technologies for the development of the pre-salt cluster, Santos basin, Brazil. In: Offshore Technology Conference. Proceedings. Texas: OTC; 2009. p. OTC-19880.
42. Pereira HB, Moreira MF, de Almeida NL, Batista IP. Influence of stress and temperature on stress corrosion cracking of welded duplex stainless steel joints under drop evaporation test. In: CORROSION 2019. Proceedings. Tennessee: Nace Corrosion; 2019. p. 13420.
43. Zhu YX, Song GL, Wu PP, Huang JF, Zheng DJ. A protective superhydrophobic Mg–Zn–Al LDH film on surface-alloyed magnesium. J Alloys Compd. 2021;855(2):157550.
44. Silva RG, Vieira MR, Malta MIC, Silva CH, Oliveira SH, Urtiga SL. Filho. Effect of initial surface treatment on obtaining a superhydrophobic surface on 5052 aluminum alloy with enhanced anticorrosion properties. Surf Coat Tech. 2019;369:311-22.
45. Malta MIC, Vieira MRS, Silva RGCD, Silva LMCD, Araújo EGD, Maciel SHDO, et al. Superhydrophobic Surfaces on 5052 Aluminum Alloy Obtained from LDH film modified with stearic acid for enhanced corrosion protection. Mater Res. 2019;22(6):20180882.
46. Hang T, Hu A, Ling H, Li M, Mao D. Super-hydrophobic nickel films with micro-nano hierarchical structure prepared by electrodeposition. Appl Surf Sci. 2010;256(8):2400-4.
47. Wang S, Shi J, Liu C, Xie C, Wang C. Fabrication of a superhydrophobic surface on a wood substrate. Appl Surf Sci. 2011;257(22):9362-5.
48. Mail M, Klein A, Bleckmann H, Schmitz A, Scherer T, Rühr PT, et al. A new bioinspired method for pressure and flow sensing based on the underwater air-retaining surface of the backswimmer Notonecta. Beilstein J Nanotechnol. 2018;9(1):3039-47.
49. Bing W, Wang H, Tian L, Zhao J, Jin H, Du W, et al. Small structure, large effect: functional surfaces inspired by salvinia leaves. Small Structures. 2021;2(9):2100079.
50. Barthlott W, Moosmann M, Noll I, Akdere M, Wagner J, Roling N, et al. Adsorption and superficial transport of oil on biological and bionic superhydrophobic surfaces: a novel technique for oil–water separation. Philosophical Transactions of the Royal Society A. 2020;378(2167):20190447.
51. Zeiger C, da Silva ICR, Mail M, Kavalenka MN, Barthlott W, Hölscher H. Microstructures of superhydrophobic plant leaves-inspiration for efficient oil spill cleanup materials. Bioinspir Biomim. 2016;11(5):056003.
52. Ribeiro TH, Rubio J, Smith RW. A dried hydrophobic aquaphyte as an oil filter for oil/water emulsions. Spill Sci Technol Bull. 2003;8(5-6):483-9.
53. Zhang X, Hu C, Lin J, Yin H, Shi J, Tang J, et al. Fabrication of recyclable, superhydrophobic-superoleophilic quartz sand by facile two-step modification for oil-water separation. J Environ Chem Eng. 2022;10(1):107019.
54. Parsaie A, Tamsilian Y, Pordanjani MR, Abadshapoori AK, McKay G. Novel approach for rapid oil/water separation through superhydrophobic/superoleophilic zinc stearate coated polyurethane sponges. Colloids Surf A Physicochem Eng Asp. 2021;618:126395.
55. Seth M, Khan H, Bhowmik R, Karmakar S, Jana S. Facile fabrication of fluorine free zirconium zinc stearate based superhydrophobic and superoleophilic coating on cotton fabric with superior antibacterial property. J Sol-Gel Sci Technol. 2020;94:127-40.